The Astrophysical Journal, 734:30 (9pp), 2011 June 10 doi:10.1088/0004-637X/734/1/30

MULTI-FLUID MODEL OF A STREAMER AT SOLAR MINIMUM AND COMPARISON WITH OBSERVATIONS

Leon Ofman[1,3], Lucia Abbo[2], and Silvio Giordano[2]
[1] Department of Physics, The Catholic University of America, and NASA Goddard Space Flight Center, Code 671, Greenbelt, MD 20771, USA; Leon.Ofman@nasa.gov
[2] INAF Astronomical Observatory of Turin, Italy
Received 2010 November 9; accepted 2011 March 29; published 2011 May 23

ABSTRACT

We present the results of a time-dependent 2.5-dimensional three-fluid magnetohydrodynamic model of the coronal streamer belt, which is compared with the slow solar wind plasma parameters obtained in the extended corona by the UV spectroscopic data from the Ultraviolet Coronagraph Spectrometer (UVCS) on board *SOHO* during the past minimum of solar activity (Carrington Rotation 1913). Our previous three-fluid streamer model has been improved by considering the solar magnetic field configuration relevant for solar minimum conditions, and preferential heating for O^{5+} ions. The model was run until a fully self-consistent streamer solution was obtained in the quasi-steady state. The plasma parameters from the multi-fluid model were used to compute the expected UV observables from H I Lyα 1216 Å and O VI 1032 Å spectral lines, and the results were compared in detail with the UVCS measurements. A good agreement between the model and the data was found. The results of the study provide insight into the acceleration and heating of the multi-ion slow solar wind.

Key words: solar wind – Sun: corona – Sun: magnetic topology – Sun: UV radiation

Online-only material: color figures

1. INTRODUCTION

The solar wind plasma consists of three main particle species: electrons, protons, and He^{++}. In addition, the solar wind plasma contains numerous heavy ion species, such as Fe, O, etc., that emit radiation in the visible, UV, and extreme ultraviolet (EUV) that were measured by ground-based (in the visible spectral range) and space-based imaging and spectroscopic instruments such as *SOHO*/Ultraviolet Coronagraph Spectrometer (UVCS) and SUMER (in the UV and EUV). Observations by the UVCS instrument of the H I Lyα 1216 Å and O VI 1032 Å emission in the EUV showed that heavy ions such as O^{5+} are much hotter and flow faster than protons (Kohl et al. 1997; Li et al. 1998; Cranmer et al. 1998).

The heavy ion structure of the corona at solar minimum differs considerably from the structure seen in white light and hydrogen emission (Kohl et al. 1997; Raymond et al. 1997). During solar minimum the corona is dominated by a global dipolar magnetic structure with a long-lived (quiescent) streamer structure with a lifetime of several days or longer (e.g., Giordano & Mancuso 2008). Quiescent streamers show depletion of O VI ion emission in the core of the streamers, while active region streamers associated with dynamic (i.e., with constantly changing fields and flows on a timescale smaller than the streamer lifetime) small-scale coronal structures do not show this property (Strachan et al. 2002; Marocchi et al. 2001; Uzzo et al. 2003; Akinari 2007). However, the interpretation of the remote-sensing observations requires theoretical modeling in order to eliminate ambiguities inherent in the remote-sensing data (i.e., line-of-sight integration, non-thermal versus thermal contribution to spectral lines, density filling factors, lack of direct magnetic field measurements in the corona, etc.). Global single-fluid magnetohydrodynamic (MHD) models of the solar wind can provide the general streamer magnetic structure (Mikić et al. 1999), but cannot describe the different properties of the various ions.

In the weakly collisional solar wind plasma, the electrons, protons, and heavy ions can be modeled as coupled magnetized fluids using MHD-like equations. The multi-fluid model contains important physical processes, such as collisional and electromagnetic coupling between the various fluids, as well as different heating and acceleration processes for the electrons, protons, and heavy ions. These processes have not been included in past single-fluid MHD models (e.g., Mikić et al. 1999; Usmanov et al. 2000; Powell et al. 2003). Recently, the global three-dimensional MHD models were extended to include more realistic thermodynamics (e.g., Downs et al. 2010). However, the distinct dynamics and coupling of protons, electrons, and heavy ions cannot be modeled self-consistently with single-fluid models. Three-dimensional multi-ion fluid models were developed and applied to the interaction of the solar wind with solar system bodies (e.g., Liu et al. 1999; Ma et al. 2007; Toth et al. 2010). Recent three-fluid coronal streamer models were successful in reproducing the heavy ion and proton outflow and density structure of the slow solar wind (Ofman et al. 2000; Ofman 2004a; Li et al. 2006; Labrosse et al. 2006). The oxygen ion outflow in streamers was also calculated as a perturbation fluid on the top of single-fluid MHD solution (Chen et al. 2004). However, the temperature structure of oxygen ions in streamers was not considered. The fast solar wind driven by a spectrum of Alfvén waves in coronal holes was modeled as well with a three-fluid 2.5-dimensional model (Ofman & Davila 2001; Ofman 2004b), see the recent review by Ofman (2010).

In the present study of the slow wind, we focus on modeling the latitudinal structure of heavy ion density and temperature, and on comparing the model results to *SOHO*/UVCS observations (e.g., Kohl et al. 1997; Raymond et al. 1997; Abbo et al. 2010a). During solar minimum the corona can be described well by a streamer belt associated with a tilted dipole magnetic configuration. As evident from recent National Solar Observatory (NSO) and *STEREO* three-dimensional reconstruction of

[3] Visiting at the Department of Geophysics and Planetary Sciences, Tel Aviv University, Tel Aviv, Israel.

electron density, the streamer is confined to the central part of the tilted dipole (Kramar et al. 2009; Zhao & Hoeksema 2010). The first attempts of comparison between the multi-ion solar wind and the three-fluid models were recently carried out by Abbo et al. (2010b) and Ofman & Kramar (2010). We present the results of comparison between the slow solar wind plasma parameters obtained in the extended corona by the UV spectroscopic data from UVCS and an improved multi-fluid model that is guided by observations and used to calculate the H I Lyα and O VI intensity maps.

2. OBSERVATIONAL MOTIVATION

Observations show that during the minima of solar activity the slow solar wind is detected close to the ecliptic plane at 1 AU and is associated with the heliospheric streamer belt (e.g., McComas et al. 2000). During periods of high solar activity (solar maximum), the solar corona is dominated by streamers as evident from eclipse and coronagraph observations (Woo 2007; Morgan & Habbal 2010). In situ observations by the *Ulysses* spacecraft of the solar wind at solar maximum beyond 1 AU show that it is dominated by the slow solar wind in and out of the ecliptic plane (McComas et al. 2003). Some studies indicate that the slow solar wind may also be associated with coronal active regions (Woo & Habbal 2005). UVCS observations show that the appearance of coronal streamers in minor ion emission lines is significantly different compared to neutral hydrogen Lyα emission (Kohl et al. 1997; Noci et al. 1997; Raymond et al. 1997). The structure of the streamer as seen in heavy ion emission varies depending on the streamer location and dynamics (i.e., whether it is a quiescent or variable streamer on a timescale shorter than the streamer lifetime). The details of the streamer structure as seen in UV spectroscopic observations (e.g., Marocchi et al. 2001; Strachan et al. 2002; Uzzo et al. 2003; Antonucci et al. 2005; Noci & Gavryuseva 2007; Ko et al. 2008; Abbo et al. 2010a) can be explained only by considering a multi-fluid model (Ofman et al. 2000; Ofman 2004a). The white-light observations from LASCO on board *SOHO* have shown numerous small blowouts which are carried by the slow solar wind within the streamer belt and were used to measure the slow solar wind outflow velocity profile (e.g., Sheeley et al. 1997; Wang et al. 1998). More recently, the *STEREO*/Heliospheric Imagers (HI) data have revealed a plethora of small-scale solar transients flowing outward from the Sun into the heliosphere (Davies et al. 2009), which can represent the same phenomena as observed with LASCO.

The goals of the present study are reproducing and better understanding the observationally deduced (with significant error bars) latitudinal and radial dependence of the O^{5+} ion temperature, the different (from O^{5+}) latitudinal dependence of the proton and electron temperatures, the lower values of the proton and electron temperatures compared to the O^{5+} ion temperature, the magnetic topology of the streamer at solar minimum, the different latitudinal variation of the density of protons and oxygen ions in streamers at solar minimum (as deduced from H I and O VI emission lines), and the typical observed outflow speed of the slow solar wind in streamers at solar minimum. For this purpose we develop the three-fluid model described below.

The planned NASA *Solar Probe Plus* mission will measure in situ plasma composition in the inner corona, and at closest approach at about 9.5 $R_\odot$ will provide information on the parameters of streamer plasma (McComas et al. 2008). Moreover, the European *Solar Orbiter* mission will provide plasma measurements in the inner corona. Since models show (e.g., Chen et al. 2003) that the ionic composition is frozen-in beyond about 1.2–2 $R_\odot$, the results of multi-fluid model such as the one described below provide as output the multi-ion slow solar wind outflow in these regions and can be used for planning and interpreting the in situ observations in the inner corona.

3. THREE-FLUID MODEL EQUATIONS

We develop a 2.5-dimensional multi-species model with azimuthal symmetry (i.e., two spatial dimensions and three components of velocities and of the magnetic field) of the streamers that helps better understand the physics of the slow solar wind, better match existing heavy ion observations, as well as predict the structure of the streamers in yet unobserved ions. The three-fluid equations are obtained by neglecting electron inertia (i.e., using $m_e \ll m_p$ to solve the electron momentum equation for the electric field), relativistic effects ($V \ll c$), and heat conduction, assuming quasi-neutrality ($n_e = n_p + Zn_i$), where Z is the charge number, and neglecting viscosity the normalized three-fluid MHD equations are

$$\frac{\partial n_k}{\partial t} = -\nabla \cdot (n_k \mathbf{V}_k), \tag{1}$$

$$n_k \left[\frac{\partial \mathbf{V}_k}{\partial t} + (\mathbf{V}_k \cdot \nabla)\mathbf{V}_k \right] = -E_{uk} \nabla p_k - E_{ue} \frac{Z_k n_k}{A_k n_e} \nabla p_e - \frac{n_k}{F_r r^2} \mathbf{e}_r + \Omega_k n_k (\mathbf{V}_k - \mathbf{V}_e)\mathbf{B} + \mathbf{F}_v + n_k \mathbf{F}_{k,\mathrm{coul}}, \tag{2}$$

$$\frac{\partial \mathbf{B}}{\partial t} = \nabla \times (\mathbf{V}_e \times \mathbf{B}) + \frac{1}{S} \nabla^2 \mathbf{B}, \tag{3}$$

$$\mathbf{V}_e = \frac{1}{n_e} (n_p \mathbf{V}_p + Z_i n_i \mathbf{V}_i - b \nabla \times \mathbf{B}), \tag{4}$$

$$\frac{\partial T_k}{\partial t} = -(\gamma_k - 1) T_k \nabla \cdot \mathbf{V}_k - \mathbf{V}_k \cdot \nabla T_k + C_{kjl} + (\gamma_k - 1)(S_k - \delta_{k,e} S_{r,e}), \tag{5}$$

where the index $k = p,\ i$ (in Equation (5) $k = e,\ p,\ i$), n_k is the density, $\mathbf{V}_k$ is the velocity, T_k is the temperature for each species, S_k is the empirical heating term, $S_{r,e}$ is the electron radiative loss term given below, $\delta_{k,e}$ is the Kronecker delta, C_{kjl} is the energy coupling term between the species (see Ofman 2004b, for detail expression), γ_k is the polytropic index of each species, A_k is the mass number, and $\Omega_k = \frac{Z_k e B_0}{A_k m_p c} \tau_A$ is the normalized gyrofrequency, where m_p is the proton mass and τ_A is the Alfvén time $\tau_A = R_\odot / V_A$, where $V_A = B_0 / \sqrt{4\pi m_p n_{e0}}$ is the Alfvén speed, B_0 is the normalization magnetic field strength, m_p is the proton mass, and n_{e0} is the normalization value (see below) of the electron number density.

In the above dimensionless equations the following normalization was used: $r \rightarrow r/R_\odot$, where $R_\odot$ is the solar radius; $t \rightarrow t/\tau_A$; $V \rightarrow V/V_A$; $B \rightarrow B/B_0$; $n_k \rightarrow n_k/n_{e0}$; $T_k \rightarrow T_k/T_{k0}$; $S = \tau_r/\tau_A$ the Lundquist number (in the present study $S = 10^4$); $\tau_r = 4\pi R_\odot^2/\nu c^2$ the resistive timescale, where ν is the resistivity and c is the speed of light; $E_{ue,p} = (k_b T_{e,p,0}/m_p)/V_A^2$ the electron or proton Euler number; $E_{ui} = (k_b T_{i,0}/m_i)/V_A^2$ the ion Euler number; $F_r = V_A^2 R_\odot/(GM_\odot)$ is the Froude number, where G is the universal gravitational constant and $M_\odot$ is the solar mass; $b = cB_0/(4\pi e n_{e0} R_\odot V_A)$, $T_{k,0}$ is the temperature,

n_k is the density, m_k is the mass of particles k, and k_b is the Boltzmann constant. The 2.5-dimensional model is obtained by assuming azimuthal symmetry ($\partial/\partial\phi = 0$) in the above equations. In the present study we use $B_0 = 7$G, $n_{e0} = 5\times10^8$ cm^{-3}, $T_{e0} = T_{p0} = 1.6$ MK, and $T_{i0} = 32$ MK. The Coulomb friction terms $\mathbf{F}_{k,\mathrm{coul}}$ are given by Braginskii (1965; see Ofman 2004b for the detailed form of these terms).

Note that by substituting the electron velocity $\mathbf{V}_e$ given by Equation (4) in the Lorentz force term in Equation (2), this term can be written as

$$\Omega_k n_k(\mathbf{V}_k - \mathbf{V}_e)\times\mathbf{B} = \Omega_k\frac{n_k}{n_e}(n_e\mathbf{V}_k - n_p\mathbf{V}_p - Z_i n_i\mathbf{V}_i)\times\mathbf{B} + b\Omega_k\frac{n_k}{n_e}(\nabla\times\mathbf{B})\times\mathbf{B}. \quad (6)$$

The first term on the right-hand side of Equation (6) describes the gyromotion of the proton and ion fluids, and the second term on the right-hand side is the force produced by the partial currents due to each ion–electron fluid relative motion. For the present slow solar wind study waves are neglected, and in the low-frequency regime ($\omega \ll \Omega_p$), or when collisions are dominant ($\Omega_p \ll \nu_p$, where ν_p is the proton collision frequency) the gyromotion term can be neglected (Gan-Baruch et al. 1998; Ofman et al. 2000). Thus, one can approximate

$$\Omega_k n_k(\mathbf{V}_k - \mathbf{V}_e)\times\mathbf{B} \approx \frac{Z_k}{A_k}(\nabla\times\mathbf{B})\times\mathbf{B} \quad (7)$$

by neglecting the high-frequency gyroresonant term on the right-hand side in Equation (6) and substituting $b\Omega_k\frac{n_k}{n_e} = \frac{Z_k}{A_k}$. This allows solving the above equations explicitly with a time step not limited by the short gyroresonant timescales.

In the present study, the energy equation is simplified by assuming a polytropic index $\gamma_k = 1.05$, neglecting explicit heating terms for electrons and protons. The electron heat conduction is high in the corona due to the high temperature of the coronal plasma heated by (not fully understood) mechanism that balances conductive and radiative losses and the dependence of the heat conduction on electron temperature $\sim T_e^{5/2}$ (Spitzer 1956). This results in a nearly isothermal structure of the inner corona. The inclusion of explicit electron heat conduction term in the energy equation is numerically challenging and was only attempted in a few studies of streamers (for example, see Cuperman et al. 1990; Stewart & Bravo 1997). Recently, progress has been made in including these terms in global three-dimensional MHD models (e.g., Downs et al. 2010). The form of the collisional (Spitzer 1956) electron heat conduction term is likely not applicable beyond ~2 solar radii above the photosphere, due to the rapid decrease in electron collision frequency. Since the exact physical mechanism that heats the corona is unknown, the heating term can only be estimated empirically (Guhathakurta et al. 2006; Airapetian et al. 2011). Alternatively, the polytropic index can be adjusted empirically with height to match observed quantities (Cohen et al. 2007). The value $\gamma = 1.05$ is commonly used in global MHD models of the solar wind and is known to reproduce only qualitatively the properties of the solar wind (e.g., Mikić et al. 1999). However, the energy equation in the present model contains additional terms: the energy exchange terms C_{jkl} couple the temperatures of the species, where collisions are important, and a simplified radiative loss term is important close to the Sun of the form $S_e = a_e n_e T_e^{-1}$, where $a_e = n_{e0}\xi\, R_\odot/(2V_A k_b T_{e0}^2)$ with present normalization and $\xi = 5.51\times10^{-17}$ erg s^{-1} cm^3 is the constant

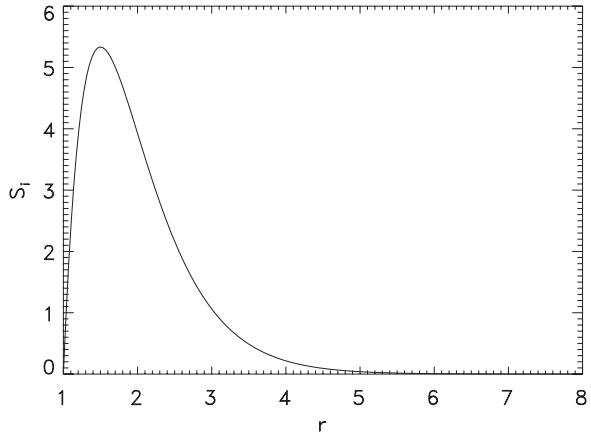

Figure 1. Radial dependence of the O^{5+} heating function used in the three-fluid model (Equation (8)).

appropriate for coronal temperature range (Rosner et al. 1978). For O^{5+} ions the following spherically symmetric heating term is included (see Figure 1):

$$S_i = S_{i0}(r-1)e^{-(r-1)/\lambda_{i0}}, \quad (8)$$

where the constants S_{i0} and λ_{i0} determine the magnitude and the decrease of the heating rate with distance. These parameters were fit to match the radial dependence of the O^{5+} temperature, as described below.

3.1. Boundary, Initial Conditions, and Method of Solutions

The 2.5-dimensional model in spherical geometry is obtained by assuming azimuthal symmetry ($\partial/\partial\phi = 0$) in the above equations, while keeping all three components of the velocity and the magnetic field. The following boundary conditions are applied at the lower boundary at $r = 1\,R_\odot$: $\mathbf{B}(r,\theta) = \mathbf{B}_0(1,\theta)$, where $\mathbf{B}_0(1,\theta)$ is the dipole field. In addition, $B_\phi = V_{k,\phi} = 0$ and the variables n, T_k, $V_{k,r}$, $V_{k,\theta}$ are extrapolated from the interior points to the boundary, approximating incoming characteristics. At $\theta = (0,\pi)$ and at $r = r_{\max}$ open boundary conditions are used, i.e., the values of the variables at the open boundaries are extrapolated from interior points.

The dipole field $\mathbf{B}_0 = \frac{1}{r^3}(2\cos\theta,\ \sin\theta)$ is used as the initial magnetic field in the computational domain (see Figure 2). The $V_{p,r}$ and n_p are initialized with Parker's isothermal solar wind solution with $T = 1.6$ MK (Parker 1963), thus imposing a subsonic solar wind flow at $r = 1\,R_\odot$ and a supersonic solar wind flow at the outer boundary in the initial state. The initial O^{5+} density is taken as $8\times10^{-4}n_p$ at $r = 1\,R_\odot$ with a hydrostatic distribution with height at an initially uniform O^{5+} temperature $T_{O^{5+}} = 32$ MK. The initial flow is not consistent with an initial dipole field. However, the solution evolves quickly (within $< 50\tau_A$) to a self-consistent streamer solution with open and closed field regions. The density, temperature, and velocity of protons and O^{5+} adjust, reach the steady-state values self-consistently everywhere, including at the boundaries (see the following section).

The equations are solved using fourth-order Runge–Kutta method in time and fourth-order spatial differencing with typical resolution of 320×516. Chebyshev fourth-order smoothing term is applied for stability. The code is parallelized using the Message Passing Interface with efficient solution on 128 processors.

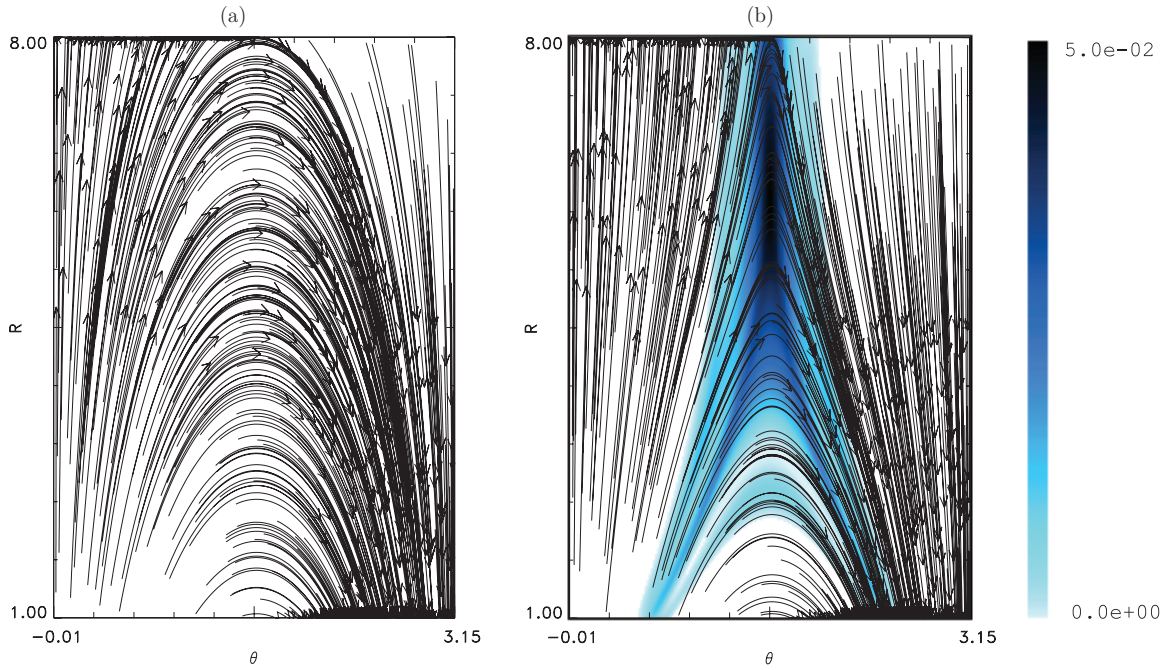

Figure 2. Magnetic field lines of (a) an initial dipole field (current-free) used in the present model at $t = 0$ and (b) a streamer at the end of the run ($t = 68.1\tau_A$) calculated with the three-fluid model. The quantity j^2/ρ shows the location of the current sheet (blue scale) formed with the streamer.

(A color version of this figure is available in the online journal.)

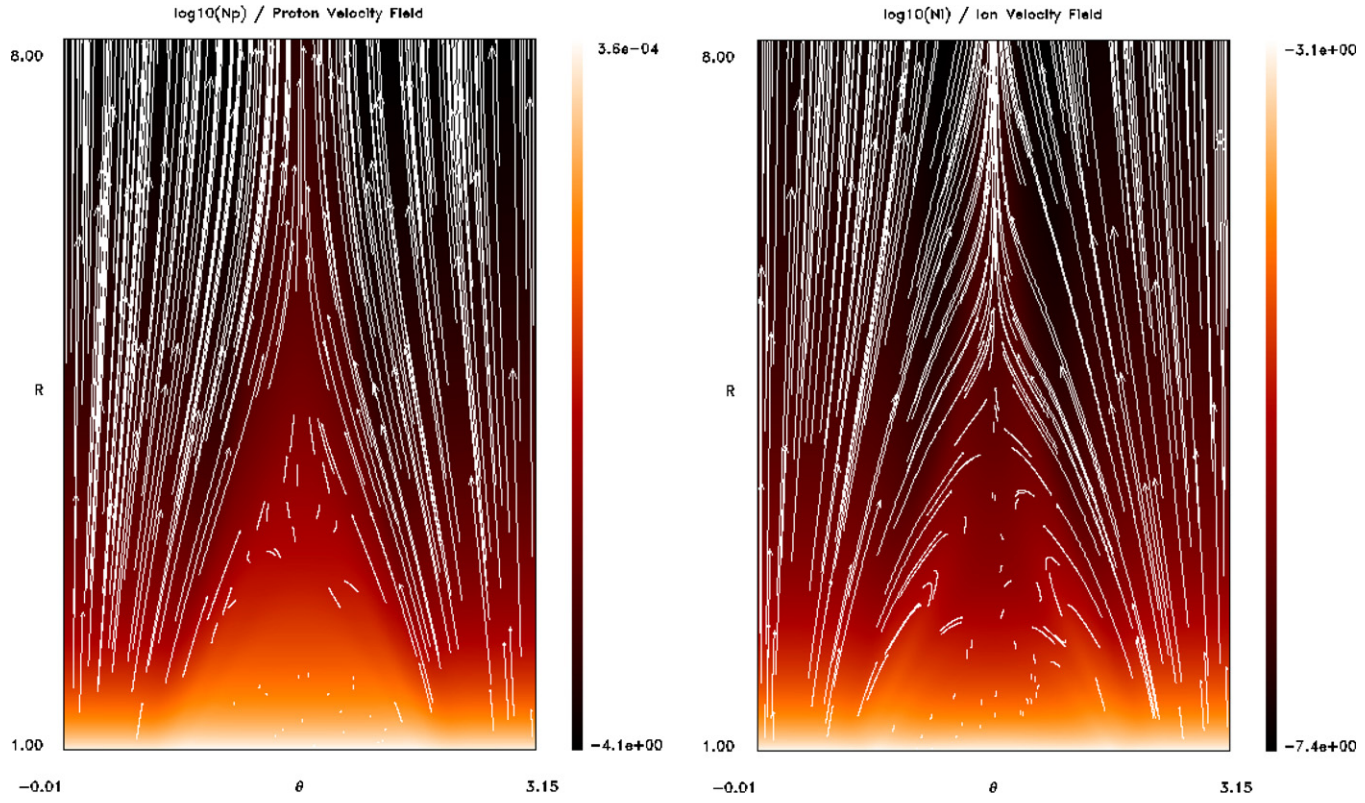

Figure 3. Density structure of protons and O^{5+} ions (shown on logarithmic scale) overlaid with proton and O^{5+} ion velocity streamlines at $t = 68.1\tau_A$. The density is in units of 5×10^8 cm^{-3}.

(A color version of this figure is available in the online journal.)

4. NUMERICAL RESULTS

In Figures 2–5 the results of the three-fluid simulation of streamer formation with electrons, protons, and O^{5+} ions are shown. The parameters of the O^{5+} ion heating function are $S_{i0} = 29.0$ and $\lambda_{i0} = 0.5$. These parameters were optimized to match the observed radial dependence of the O^{5+} temperature, and it was found that the typical damping length of the heating is $0.5\,R_\odot$ (i.e., $\lambda_{i0} = 0.5$). The heavy ions were initially in hydrostatic equilibrium. By the end of the run heavy ion outflow

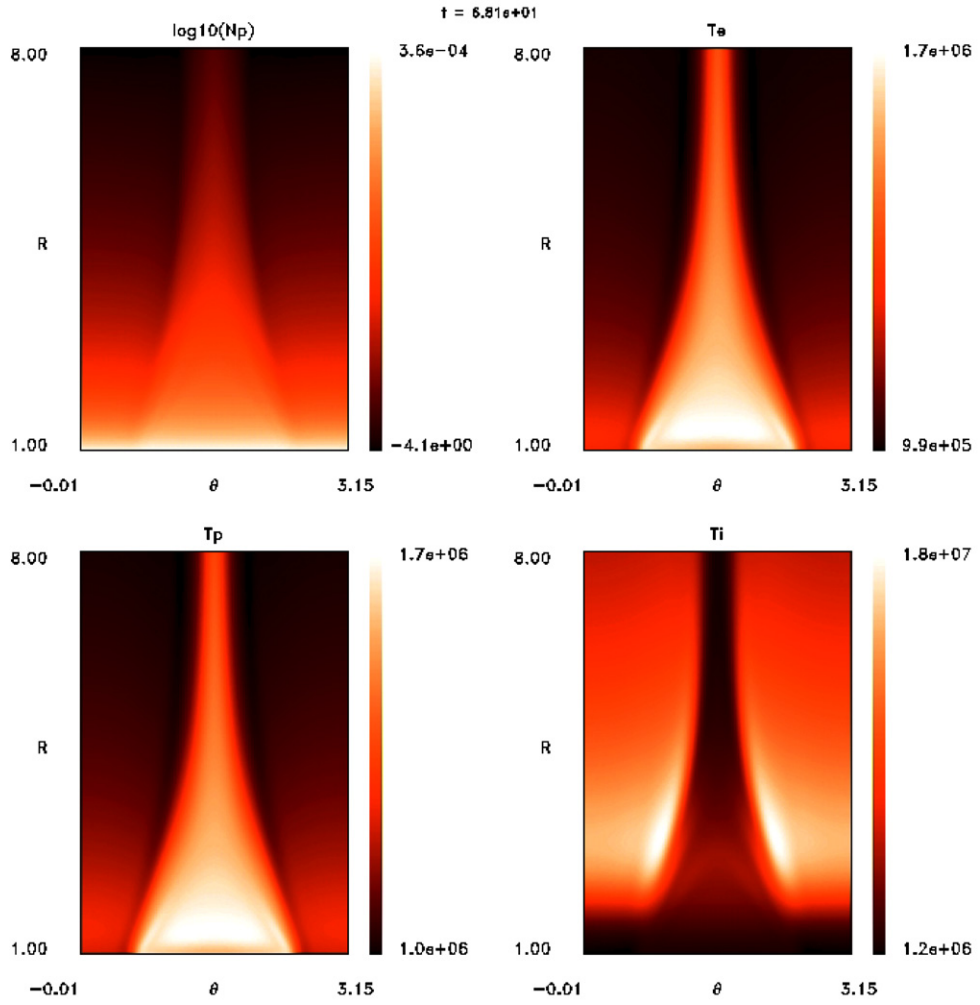

Figure 4. Streamer proton density structure and temperatures of electrons, protons, and O^{5+} ions at $t = 68.1\tau_A$.
(A color version of this figure is available in the online journal.)

has formed in open field regions, and the temperature of the ions decreased and became radially and latitudinally non-uniform due to energy and momentum exchange with electrons and protons and heating introduced in the model equations.

In Figure 2 the initial and the final magnetic field of the streamer are shown. At $t = 0$ the magnetic field is a potential dipole field in the half-plane (Figure 2(a)). At the end of the run when the solution has reached a quasi-steady state, a streamer has formed with closed and open field regions separated by the current sheets (Figure 2(b)). The proton and O^{5+} velocities became large in the open field region, compared to the velocities in the closed field region (see Figure 5 below).

In Figure 3 the density structure of protons and O^{5+} ions is shown overlaid with proton and O^{5+} velocity streamlines at $t = 68.1\tau_A$. At this time the solutions are in the quasi-steady-state regime, slowly varying in time compared to the initial variation timescale. This is tested by inspecting the temporal evolution of the solutions overall through animations of the streamer density, field, and flow, and in detail by noting the decrease of the temporal gradients of the solutions at several representative points in the computational domain. It is evident that the proton density is largest at the core of the streamer, while the O^{5+} density peaks near the boundary of the regions that separate open and closed field regions. Since the O^{5+} ions are heavier than protons, their gravitational scale height is smaller than the proton fluid gravitational scale height (taking into account the polarization electric field due to plasma quasi-neutrality and gravity, e.g., Lenz 2004) in the core of the streamer at similar temperatures, resulting in their gravitational settling. The O^{5+} ion gravitational settling can take place since the protons are nearly static in this region. In the open field region the initially hydrostatic ion structure has changed to outflowing, as the O^{5+} ions are carried by the outflowing protons due to Coulomb friction. At the outer boundary (8 $R_\odot$), the solar wind speed reaches 164 km s^{-1} for O^{5+} ions and 198 km s^{-1} for protons. Note that, higher velocities, characteristic of the fast solar wind, are not produced by the model since this model includes the physical processes leading to slow wind only (i.e., momentum addition terms required for fast wind modeling are not included). The outflow speed of the slow solar wind protons obtained in this model is close to the bulk solar wind outflow speed (due to the low abundance O^{5+} ions), and we find that this speed is in good agreement with LASCO measurements of the bulk solar wind outflow as determined from observations of outflow of small-scale structures (e.g., Sheeley et al. 1997).

In Figure 4 the streamer proton density structure and temperatures of electrons, protons, and O^{5+} at $t = 68.1\tau_A$ are shown. It is evident that the electron and proton temperatures peak at the core of the streamer, while the O^{5+} temperature peaks outside the streamer core. The latitudinal variation of the temperatures

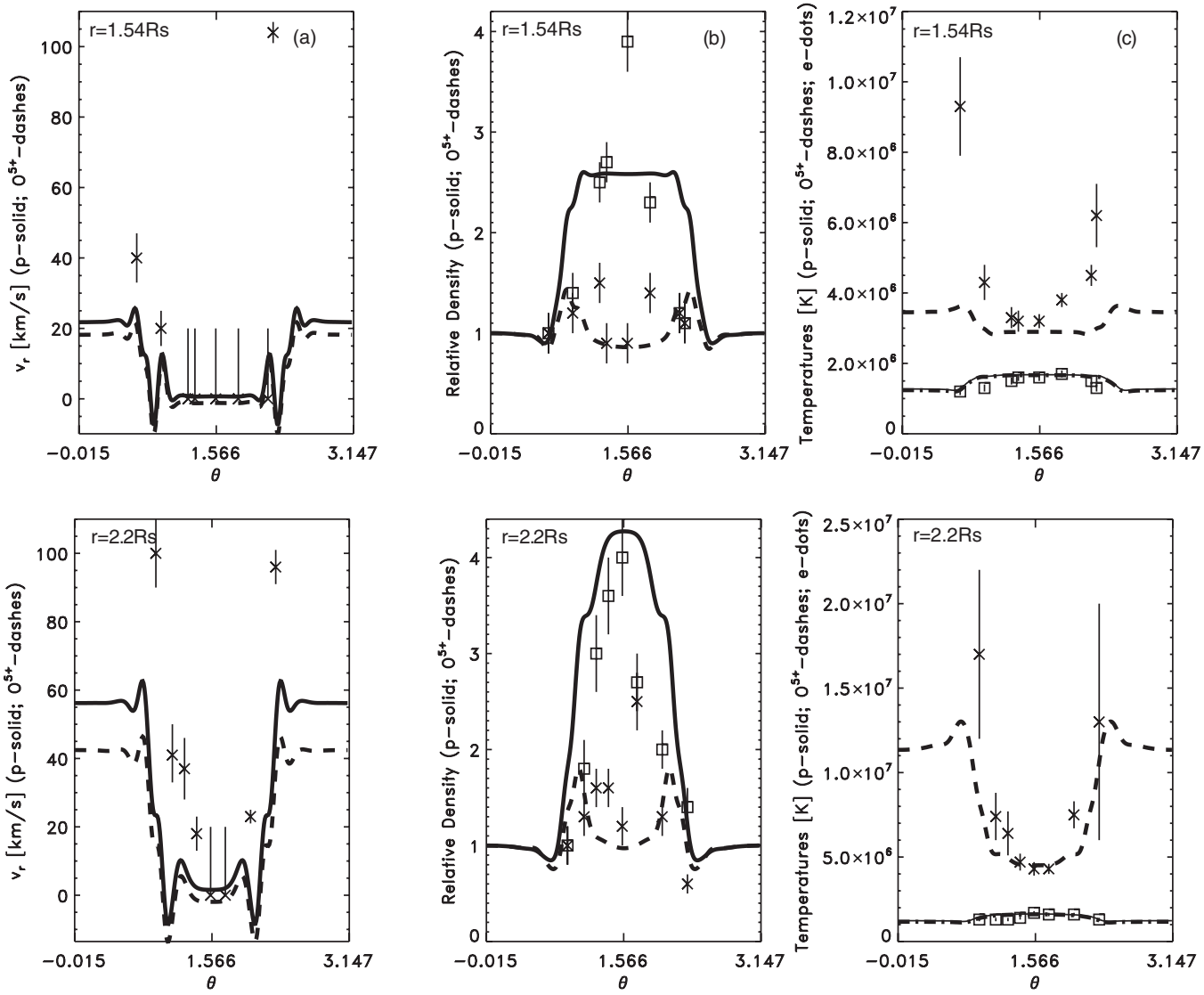

Figure 5. θ dependence of (a) velocities, (b) densities, (c) temperatures for protons (solid), O^{5+} ions (dashes), and electrons (dot dashes) at $r = 1.54\,R_\odot$ (top panels) and $r = 2.2\,R_\odot$ (bottom panels) obtained from the three-fluid model. The observational values derived from UVCS data (1996 August 29–September 1; Abbo et al. 2010a) are marked with error bars (crosses for O^{5+} ions and squares for neutral hydrogen atoms).

reflects the latitudinal magnetic and density structure of the streamer. The initially uniform temperatures were affected by the magnetic field structure, the interaction between the species, and the small radiative cooling in the core of the streamer. The heating function (Equation (8)) was applied only to O^{5+} ions and varies only in the radial direction. The parameters of the heating functions were optimized to fit the radial dependence of the O^{5+} temperature as deduced from observation (see Figure 5 below). Nevertheless, both radial and latitudinal variations of the O^{5+} ion temperature are produced by the model. This is due to the cooling of O^{5+} ions in the core of the streamer due to Coulomb energy exchange with electrons and protons.

4.1. Latitudinal Variation: Comparison to Observations

Detailed latitudinal variations of the proton and O^{5+} ion velocities, densities, and temperatures obtained with the three-fluid model are shown in Figure 5, at $r = 1.54\,R_\odot$ and $r = 2.2\,R_\odot$. The symbols with error bars (crosses for O^{5+} ions and squares for neutral hydrogen atoms) show the observational values derived from UVCS data (1996 August 29–September 1), which have been analyzed by Abbo et al. (2010a). The central latitude of the observed streamer was shifted to the center of the dipole, and the width of the streamer is in good agreement with the model streamer. It is evident that the density structure and temperatures agree well with observations at the two heights. In the core of the streamer the proton and ion velocities are small (the absolute value of the velocity is $\sim$1 km s^{-1} at height of $1.54\,R_\odot$ and $\sim$2 km s^{-1} at height of $2.2\,R_\odot$ in the center of the streamer). The small velocity in the core is consistent with UVCS velocity measurement. In the open field region, the ion velocity is 18 km s^{-1} and proton velocity is 20 km s^{-1} at $1.54\,R_\odot$, and 42 km s^{-1} and 56 km s^{-1} at $2.2\,R_\odot$, respectively. The proton velocity values are in qualitative agreement with LASCO measurements that measure the bulk solar wind outflow (Sheeley et al. 1997). However, the O^{5+} outflow velocity values obtained from the model are lower than the values obtained from UVCS using the Doppler dimming effect ($\sim$100 km s^{-1} at both heights). Since these points are outside the streamer, the high speeds are likely due to the contribution from fast wind streams. The cross-sectional density is normalized by the density value at the left boundary. It is evident that the O^{5+}

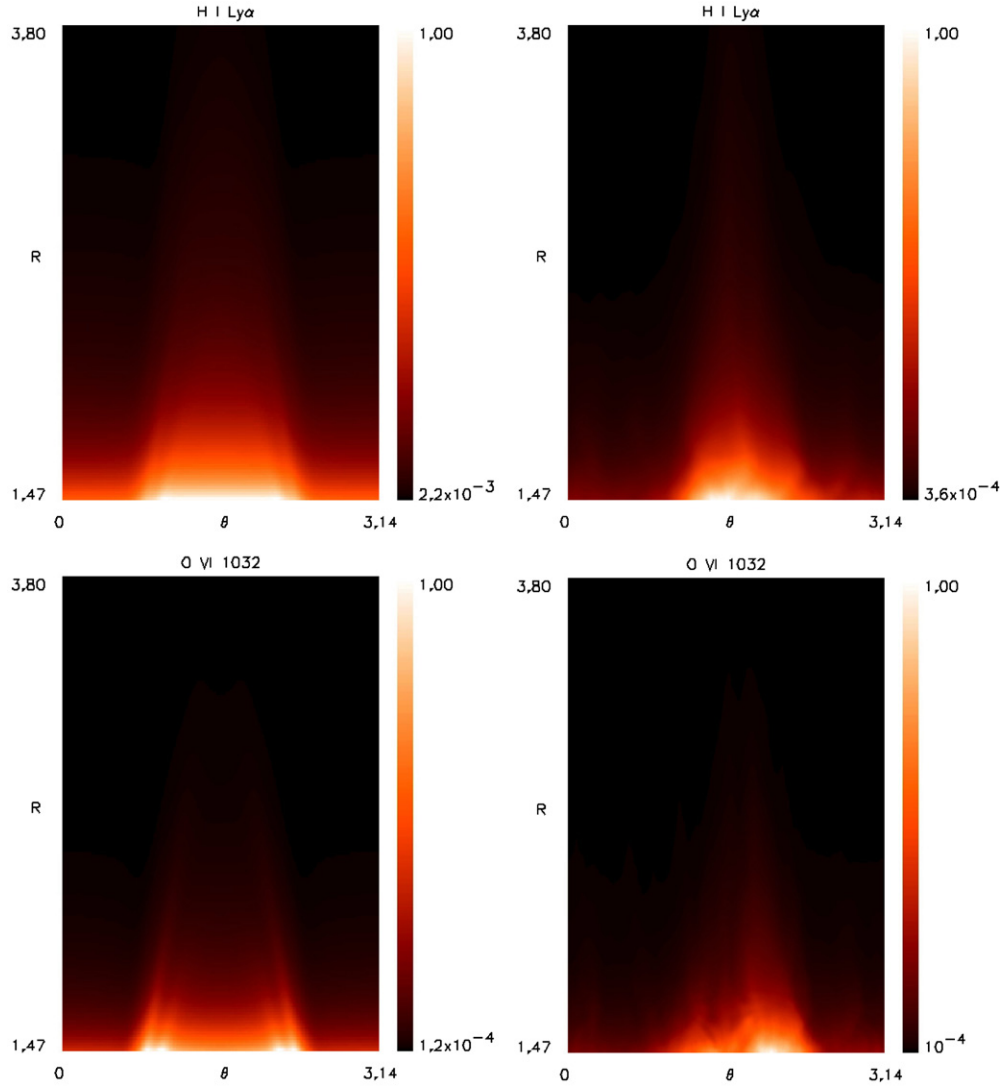

Figure 6. Left: H I Lyα (top) and O VI 1032 Å (bottom) simulated intensity maps obtained from the results of the three-fluid model (in relative units). Right: H I Lyα (top) and O VI 1032 Å (bottom) interpolated and normalized intensity maps, from 1996 August 25–September 1 UVCS data.

(A color version of this figure is available in the online journal.)

density peaks near the boundary of the streamer, while the proton density peaks at the core at the two heights. The proton density results from the model match the proton density values (squares in Figure 5(b)) derived from UVCS determinations of electron density (Abbo et al. 2010a) with the assumption of a coronal plasma with 10% of helium abundance. The ion density peaks are in agreement with the computed oxygen density values (crosses in Figure 5(b)) derived from the proton density values, the oxygen abundance in quiescent streamer (e.g., Marocchi et al. 2001), and the ionization fraction of the O VI ions (Arnaud & Rothenflug 1985) by considering the small variation of the electron temperature across the streamer (see Figure 4).

The latitudinal dependence of the electron, proton, and O^{5+} ion temperature is shown in Figure 5(c). The electron and proton temperatures are nearly equal, peaking at the core of the streamer, and their variation with height is weak due to the nearly isothermal ($\gamma_e = \gamma_p = 1.05$) polytropic energy equations. The O^{5+} ions are subject to radially dependent heating and cooling due to interaction with electrons and protons. The resulting $T_{O^{5+}}$ increases with height and is lowest in the core of the streamer. The temperature variation is in good agreement with UVCS observational data points. The highest O^{5+} temperature is observed outside the streamer with likely contribution from coronal hole plasma.

4.2. Computation of Intensity Maps

The parametric description of the solar corona obtained by the 2.5-dimensional three-fluid MHD model is used to compute the expected emissivity in the plane of the sky from H I Lyα and O VI 1032 Å spectral lines. The emissivity structure provides qualitative representation of the total intensity without assumptions about the coronal geometry along the line of sight, thus allowing unbiased comparison between the model results and the spectral emissions observed by UVCS. The multi-fluid model provides maps of values for a full set of coronal parameters, such as temperatures, densities, and ion outflow velocities which enables the computations of maps of UV emission from the solar corona. There are two main mechanisms contributing to the formation of a UV coronal line: the resonant scattering of radiation coming from the bright solar disk by ions in the outer corona and the collisional excitation by

electron impact on ions followed by radiative decay. Therefore, the total emissivity coming from an optically thin corona is the combination of the resonant, $j_{\rm res}$, and collisional, $j_{\rm coll}$, emissivities:

$$j = j_{\rm res} + j_{\rm coll}. \quad (9)$$

Following Noci et al. (1987), the two components are given by

$$j_{\rm res} = \frac{b_r B_{1k}\, h\, \lambda_{1k}}{4\pi} n_i \int_\Omega p(\phi)\, d\omega \int_0^{+\infty} I_{ex}(\lambda - \delta\lambda)\, \Phi(\lambda, \mathbf{n}')\, d\lambda \quad (10)$$

and

$$j_{\rm coll} = \frac{b_r}{4\pi} n_e n_i q_{1k}(T_e), \quad (11)$$

where b_r is the branching ratio, λ_{1k} is the reference wavelength of considered transition, n_e and n_i are the electron and ion density, respectively, $p(\phi)$ takes into account the geometry of the scattering process, and ϕ is the angle between the direction of the incident radiation $\mathbf{n}'$ and the line of sight. $I_{ex}(\lambda - \delta\lambda)$ is the intensity spectrum of incident radiation from lower atmosphere, $\delta\lambda$ is the shift of this profile with respect to the reference profile due to the outflow velocity, $\mathbf{w}$, of coronal absorbing ions/atoms in the direction $\mathbf{n}'$: $\delta\lambda = \frac{\lambda_{1k}}{c}\mathbf{w}\cdot\mathbf{n}'$, $\Phi(\lambda, \mathbf{n}')$ is the coronal absorption profile, which is a function of the kinetic temperature $T_{\mathbf{n}'}$ along the direction of the incident radiation, and $q_{1k}(T_e)$ is the collisional excitation rate coefficient. In our computation we assumed uniformly bright exciting radiation coming from the solar disk, in particular for H I Lyα we adopted the SUMER profile observed at solar minimum in 1996 July (Lemaire et al. 2002) and for O VI 1032 Å the intensity reported by Wilhelm et al. (1998) and the line width by Warren et al. (1997).

The H I and O VI simulated emissivities have been computed with the above expressions (9)–(11) using the plasma parameters obtained from the results of the three-fluid model of the streamer belt at solar minimum. Then the integration along the line of sight has been performed, by assuming a cylindrical symmetry, in order to derive the spectral lines intensity maps shown in the left panels of Figure 6 in relative units. The H I and O VI spectral lines west limb normalized intensity maps reconstructed from 1996 August 25 to September 1 UVCS observations are shown as comparison in the right panels. The morphological structures of the simulated and observed streamers are in good agreement. For example, the relative variation in the radial range covered by observations, that is, from 1.47 to 3.8 $R_\odot$, is the same for the simulated and the observed intensities in the streamer. In a future study, with the development of a full three-dimensional MHD model one can relax the main geometrical assumption needed for the line-of-sight emissivity integration and a quantitative numerical comparison of the spectral line intensities can be considered.

5. CONCLUSIONS

During the solar minimum the solar magnetic field is dominated by a tilted dipole, and the slow solar wind is associated with a single streamer belt, as evident from the three-dimensional reconstruction using *STEREO* and NSO data (Kramar et al. 2009). Observations show that the physical properties of slow solar wind, such as speed, density, and composition, are strikingly different from the fast wind.

UVCS observations of H I Lyα, O VI, and other minor ion emission lines in streamers such as N, S, Si, Fe, Mg, Al (e.g., Raymond et al. 1997) provide clues for the acceleration and heating mechanism, and require multi-fluid and kinetic modeling in order to interpret the results. The slow solar wind in streamers has been modeled with single-fluid two-dimensional and three-dimensional MHD codes as part of global models for decades. However, to compare the compositional properties to observations requires multi-fluid models. In this study the main properties of the slow solar wind in solar minimum streamers as seen in H I Lyα and O VI spectral lines were reproduced and the goals outlined in the observational motivation in Section 2 have been successfully achieved with the present three-fluid model as evident from the numerical results and comparison to observations (Section 4). The limitations of the model (discussed below) and the observational uncertainty can account for the quantitative differences between the observed and calculated values of the streamer physical quantities.

Observations and multi-fluid models of compositional structure of streamers reported here provide information for the first time on slow solar wind acceleration regions, O^{5+} ion heating and cooling, and the interaction between electrons, protons, and O^{5+} ions. The model includes several simplifying assumptions and uses a dipole magnetic field as the solar boundary condition. We find that the latitudinal variation of basic physical properties of streamers, such as density, temperature, and outflow speed, deduced from UVCS and LASCO observations is reproduced well with our observationally constrained multi-fluid model.

Our study leads to the conclusion that the latitudinal variation of the heavy ion temperature in a streamer is likely determined by energy exchange with electrons and protons even if the heating of heavy ions is uniform in open and closed field regions (since we have used latitudinally uniform O^{5+} ion heating function). Similarly, the latitudinal velocity and density variation of heavy ions in a streamer can be produced entirely by the interaction with outflowing electrons and protons in open field regions, and by gravitational settling of cooler heavy ions in closed field region (for example, no such latitudinal variation is seen in three-fluid models of solar wind in coronal holes in an open magnetic field structure, e.g., Ofman 2004a). The cooling of the heavy ions and heating of protons and electrons occur through the energy exchange term C_{jkl} in the energy equation. The initially uniform electron, proton, and O^{5+} ion temperatures evolved into the non-uniform (latitudinally and radially) structures, as evident in Figures 4 and 5, and the results are in agreement with observations, as evident in the reconstructed intensity maps of H I and O VI emission (Figure 6).

The main limitations of our model are the use of the radially variable empirical heating function for O^{5+} ions, the use of polytropic energy equations with $\gamma = 1.05$, the assumption of azimuthal symmetry, and the use of dipole magnetic field as the initial state. Expanding this study by including non-thermal sources, such as the spectrum of resonant and non-resonant waves, explicit electron heat conduction (with $\gamma = 5/3$) will allow studying slow solar wind acceleration and heating in multi-ion streamers with even more realistic results. This requires more complex three-fluid modeling that includes the gyroresonant terms, and explicit electron heat conduction and heating terms, adapting the recent three-fluid model developed for coronal holes (Ofman 2004b) to the more complex streamer magnetic geometry. In addition, relaxing the azimuthal symmetry assumption, and solving the full three-dimensional multi-fluid model equation, is particularly necessary when modeling the solar maximum corona that contains low-latitude as well as high-latitude streamers.

This work was supported by NASA grants NNX08AF85G and NNX08AV88G, and by NSF grant AGS-1059838. UVCS is a joint project of NASA, the Agenzia Spaziale Italiana (ASI), and the Swiss Founding Agencies. The research of L.A. has been funded through contract I/023/09/0 between the National Institute for Astrophysics (INAF) and the ASI.

REFERENCES

Abbo, L., Antonucci, E., Mikić, Z., Linker, J. A., Riley, P., & Lionello, R. 2010a, Adv. Space Res., 46, 1400
Abbo, L., Ofman, L., & Giordano, S. 2010b, in AIP Conf. Proc. 1216, Twelfth International Solar Wind Conference, ed. M. Maksimovic et al. (Melville, NY: AIP), 387
Airapetian, V., Ofman, L., Sittler, E. C., & Kramar, M. 2011, ApJ, 728, 67
Akinari, N. 2007, ApJ, 668, 1196
Antonucci, E., Abbo, L., & Dodero, M. A. 2005, A&A, 435, 699
Arnaud, M., & Rothenflug, R. 1985, A&AS, 60, 425
Braginskii, S. I. 1965, in Review of Plasma Physics, Vol. 1, ed. M. A. Leontovich (New York: Consultants Bureau), 205
Chen, Y., Esser, R., & Hu, Y. 2003, ApJ, 582, 467
Chen, Y., Esser, R., Strachan, L., & Hu, Y. 2004, ApJ, 602, 415
Cohen, O., et al. 2007, ApJ, 654, L163
Cranmer, S. R., Field, G. B., & Kohl, J. L. 1998, in ASP Conf. Ser. 154, The Tenth Cambridge Workshop on Cool Stars, Stellar Systems, and the Sun, ed. R. A. Donahue & J. A. Bookbinder (San Francisco, CA: ASP), 592
Cuperman, S., Ofman, L., & Dryer, M. 1990, ApJ, 350, 846
Davies, J. A., et al. 2009, Geophys. Res. Lett., 36, 2102
Downs, C., Roussev, I. I., van der Holst, B., Lugaz, N., Sokolov, I. V., & Gombosi, T. I. 2010, ApJ, 712, 1219
Gan-Baruch, Z., Wegmann, R., Eviatar, A., & Schmidt, H. U. 1998, J. Geophys. Res., 103, 23639
Giordano, S., & Mancuso, S. 2008, ApJ, 688, 656
Guhathakurta, M., Sittler, E. C., & Ofman, L. 2006, J. Geophys. Res., 111, 11215
Ko, Y., Li, J., Riley, P., & Raymond, J. C. 2008, ApJ, 683, 1168
Kohl, J. L., et al. 1997, Sol. Phys., 175, 613
Kramar, M., Jones, S., Davila, J., Inhester, B., & Mierla, M. 2009, Sol. Phys., 259, 109
Labrosse, N., Li, X., & Li, B. 2006, A&A, 455, 719
Lemaire, P., Emerich, C., Vial, J., Curdt, W., Schühle, U., & Wilhelm, K. 2002, in ESA Special Publication, Vol. 508, From Solar Min to Max: Half a Solar Cycle with *SOHO*, ed. A. Wilson (Noordwijk: ESA Publications Division), 219
Lenz, D. D. 2004, ApJ, 604, 433
Li, B., Li, X., & Labrosse, N. 2006, J. Geophys. Res.: Space Phys., 111, 8106
Li, X., Habbal, S. R., Kohl, J., & Noci, G. 1998, ApJ, 501, L133
Liu, Y., Nagy, A. F., Groth, C. P. T., DeZeeuw, D. L., Gombosi, T. I., & Powell, K. G. 1999, Geophys. Res. Lett., 26, 2689
Ma, Y., et al. 2007, Geophys. Res. Lett., 34, L24S10
Marocchi, D., Antonucci, E., & Giordano, S. 2001, Ann. Geophys., 19, 135
McComas, D. J., Elliott, H. A., Schwadron, N. A., Gosling, J. T., Skoug, R. M., & Goldstein, B. E. 2003, Geophys. Res. Lett., 30, 24
McComas, D. J., et al. 2000, J. Geophys. Res., 105, 10419
McComas, D. J., et al. 2008, Solar Probe Plus: Report of the Science and Technology Definition Team, NASA/TM-2008-214161 (Greenbelt, MD: NASA Goddard Space Flight Center)
Mikić, Z., Linker, J. A., Schnack, D. D., Lionello, R., & Tarditi, A. 1999, Phys. Plasmas, 6, 2217
Morgan, H., & Habbal, S. R. 2010, ApJ, 710, 1
Noci, G., & Gavryuseva, E. 2007, ApJ, 658, L63
Noci, G., Kohl, J. L., & Withbroe, G. L. 1987, ApJ, 315, 706
Noci, G., et al. 1997, Adv. Space Res., 20, 2219
Ofman, L. 2004a, Adv. Space Res., 33, 681
Ofman, L. 2004b, J. Geophys. Res., 109, A07102
Ofman, L. 2010, Living Rev. Sol. Phys., 7, 4
Ofman, L., & Davila, J. M. 2001, ApJ, 553, 935
Ofman, L., & Kramar, M. 2010, in ASP Conf. Ser. 428, SOHO-23: Understanding a Peculiar Solar Minimum, ed. S. R. Cranmer, J. T. Hoeksema, & J. L. Kohl (San Francisco, CA: ASP), 321
Ofman, L., Romoli, M., Poletto, G., Noci, G., & Kohl, J. L. 2000, ApJ, 529, 592
Parker, E. N. 1963, Interplanetary Dynamical Processes (New York: Interscience)
Powell, K. G., Gombosi, T. I., de Zeeuw, D. L., Ridley, A. J., Sokolov, I. V., Stout, Q. F., & Tóth, G. 2003, in AIP Conf. Proc. 679, Solar Wind Ten, ed. M. Velli, R. Bruno, F. Malara, & B. Bucci (Melville, NY: AIP), 807
Raymond, J. C., et al. 1997, Sol. Phys., 175, 645
Rosner, R., Tucker, W. H., & Vaiana, G. S. 1978, ApJ, 220, 643
Sheeley, N. R., Jr, et al. 1997, ApJ, 484, 472
Spitzer, L. 1956, Physics of Fully Ionized Gases (New York: Interscience)
Stewart, G. A., & Bravo, S. 1997, J. Geophys. Res., 102, 11263
Strachan, L., Suleiman, R., Panasyuk, A. V., Biesecker, D. A., & Kohl, J. L. 2002, ApJ, 571, 1008
Toth, G., Glocer, A., Ma, Y., Najib, D., & Gombosi, T. 2010, in ASP Conf. Ser. 429, Numerical Modeling of Space Plasma Flows, Astronum-2009, ed. N. V. Pogorelov, E. Audit, & G. P. Zank (San Francisco, CA: ASP), 213
Usmanov, A. V., Goldstein, M. L., Besser, B. P., & Fritzer, J. M. 2000, J. Geophys. Res., 105, 12675
Uzzo, M., Ko, Y., Raymond, J. C., Wurz, P., & Ipavich, F. M. 2003, ApJ, 585, 1062
Wang, Y., et al. 1998, ApJ, 498, L165
Warren, H. P., Mariska, J. T., Wilhelm, K., & Lemaire, P. 1997, ApJ, 484, L91
Wilhelm, K., et al. 1998, A&A, 334, 685
Woo, R. 2007, Sol. Phys., 241, 251
Woo, R., & Habbal, S. R. 2005, ApJ, 629, L129
Zhao, X. P., & Hoeksema, J. T. 2010, Sol. Phys., 266, 379